PERGAMON

International Journal of Multiphase Flow 27 (2001) 1313–1332

International Journal of Multiphase Flow

www.elsevier.com/locate/ijmulflow

Measurement of phase interaction in dispersed gas/particle two-phase flow

I. Gillandt, U. Fritsching *, K. Bauckhage

University of Bremen, Verfahrenstechnik, D-28359 Bremen, Germany

Received 15 January 2000; received in revised form 25 December 2000

Abstract

For simultaneous measurement of size and velocity distributions of continuous and dispersed phases in a two-phase flow a method is proposed and applied to increase the sensitivity of a phase-Doppler-anemometry (PDA) system. Design considerations are presented to increase the detectable size range of the PDA system to approximately 1:200 (in diameter) for simultaneous detection of tracers and particles. For this the optical properties for light scattering of the particles are properly adjusted to the measurement problem by using homogeneously coloured particles and a special signal processing procedure, which is developed to guarantee reliable signal processing of the tracer signals even with poor signal-to-noise ratios (SNR). The application of the experimental configuration is described by simultaneous measurements of gas and particle velocity and velocity fluctuation profiles in a two-phase jet arrangement with a particle diameter range from 1 (tracers) up to 160 μm (particles). In this two-phase flow at high Stokes numbers ($St \gg 1$) different turbulence structure modification effects are identified. The height of influence of these effects depends on the local position in the jet. Near the nozzle exit high gas velocity gradients exist and therefore high turbulence production in the shear layer of the jet is observed. Here the turbulence structure in the jet mainly depends on lateral turbulence transport. Due to a changed turbulence structure with reduced intensity of large eddies, this lateral transport in the two-phase jet is decreased in comparison to the single-phase jet in this area. In the area at greater nozzle distances where the jet is nearly developed, the velocity gradient in the shear layer is lower and due to this lateral turbulence transport effects become less important. Here axial turbulence transport along the jet dominates and turbulence intensity reduction is higher. © 2001 Elsevier Science Ltd. All rights reserved.

Keywords: Phase-Doppler-anemometry; Two-phase jet; Flow measurement; Phase interaction; Turbulence modulation; Turbulence analysis; Spectral analysis

* Corresponding author.
E-mail address: ufri@iwt.uni-bremen.de (U. Fritsching).

0301-9322/01/$ - see front matter © 2001 Elsevier Science Ltd. All rights reserved.
PII: S0301-9322(01)00007-6

1. Introduction

Some fluid dynamic properties in dispersed two-phase flows especially regarding particle–fluid interactions (e.g., particle dispersion and turbulence modulation) are not well understood yet. A number of previous experimental investigations are known about turbulence modulation in two-phase jets. These studies show different effects and results: Hetsroni and Sokolov (1971) measured a decrease of turbulence intensities in the two-phase jet compared to single-phase jet for Stokes numbers $St \ll 1$. For higher Stokes numbers Prevost et al. (1994), Barlow and Morrison (1990), Shuen et al. (1985) and Jou et al. (1993) measured decreased turbulence intensities in the two-phase jet compared to the single-phase jet. In contradiction to these papers Tsuji et al. (1988) presented results with decreased turbulence intensities in some measurements and increased turbulence intensities in other measurements of the two-phase jet compared to the single-phase jet. These results are ambiguous. From the aforementioned papers only Hetsroni and Sokolov (1971) – for $St \ll 1$ – and Jou et al. (1993) – for $St \gg 1$ – tried to explain the measured decrease of turbulence intensities in the two-phase jet by analysis of the turbulence structure with power-spectra measurements of the fluctuation velocity. These authors showed a decrease of turbulence energy in the high wave number region, whereas the other papers presented only statistical values showing generally decreased or increased turbulence intensities in the two-phase jet. Based on these results reduced turbulence intensities in the two-phase jet are explained as a result of turbulence energy transfer from eddies to particles following the eddies (see Tu and Fletcher, 1994). From other multiphase flow configurations turbulence analysis with energy spectra is also known. In a two-phase channel flow Kulick et al. (1994) measured the lower turbulence intensities due to a decrease of turbulence energy in the low wave number region and increased turbulence energy in the high wave number region of the two-phase flow with Stokes numbers $St \approx 1$. Schreck and Kleis (1993) measured the increased energies at the high wave number end of the spectrum in grid-generated liquid–solid flow too. These authors stated that the particles enhance the transfer of energy to smaller eddies extending the dissipation spectrum to smaller scales. The mentioned papers present results from different flow configurations and show that no general description of the driving effects and no unequivocal classification of different flow situations dependent on the driving effects are possible yet. Therefore, effects influencing turbulence modulation are still in question and because of this only some general tendencies for turbulence modulation may be summarised dependent on different flow parameters as was done by Gore and Crowe (1989), Hetsroni (1989) and Elghobashi (1994).

For an improved understanding of the turbulence modulation and its driving effects further turbulence analysis with statistical measurements of turbulence modulation and detection of the influence of the dispersed phase on the turbulence structure (e.g., by energy spectra) in the two-phase jet are necessary. Based on these measurements an improved description of the particle–fluid interaction is possible. Because of ambiguous results presented in the literature for turbulence modulation measurements in two-phase jets at higher Stokes numbers $St \gg 1$, in the present investigation this region of high Stokes numbers has been chosen to prepare and apply a proper measurement system for turbulence analysis. This measurement system should allow the description of particle–fluid interaction with rather big particles moving at high Stokes numbers. Effective description of such interaction processes is necessary in order to provide specific submodels for numerical simulation of multiphase flows. A specific need for experimental investi-

gations of phase interaction is providing fast simultaneous and correlated measurements of continuous and dispersed phases in the flow field.

For non-intrusive measurements of interactions between different particle size distributions and the turbulent carrier flow, phase-Doppler-anemometry (PDA) is a well-established method (Bauckhage, 1993). PDA is a laser-optical measurement technique for simultaneous measurement of particle velocities and sizes. This optical method detects the light scattered by an individual particle during its path through the interference volume of two intersecting laser beams. The PDA determines the particle velocity from the signal frequency shift as in conventional laser-Doppler-velocimetry (LDV) systems. If the experimental setup is well suited to the optical properties of the particles, the phase difference between two signals detected simultaneously by two detectors at different positions is proportional to the (spherical) particle diameter. Therefore, the particle diameter is determined from the phase difference of the signals.

For continuous phase measurements with LDV or PDA systems, usually the fluid is seeded with tracer particles which are size limited in a gaseous atmosphere to $d_T \approx 1$ μm in order to follow the turbulent fluctuating motion properly.

In the investigated range of particle diameters the detected light intensity scattered by the particle is proportional to the particle diameter squared ($P \sim d^2$) if transparent particles in forward scattering as in a conventional PDA setup are used. Therefore the common detectable particle diameter range is strictly limited by the receiving photomultipliers dynamic to a range of approximately 1:30. This limited particle size dynamic range of the PDA is not sufficient in many applications of dispersed two-phase flows, but especially for simultaneous measurement of both phases by detection of the described particle distribution (with $St \gg 1$) and small tracers. A wide range of, e.g., spray applications contain droplets with mean diameter of the order of 100 μm (Lefebvre, 1989). Therefore, a method for increasing the dynamic range of the PDA is needed.

In the literature several suggestions for extending the dynamic range of a PDA system have been made. Using photodiodes (Dopheide and Faber, 1989) instead of photomultipliers for scattered light detection allows higher dynamic ranges of the scattered light intensity. Also, for improved data processing accuracy of the received (low intensity) tracer and (high intensity) particle signals, a dynamic trigger has been proposed by Qiu et al. (1991). But for measurements of low intensity tracer signals, as received in a typical LDV or PDA configuration, the sensitivity of photodiodes often is not sufficient and therefore simultaneous measurements of tracers and particles in the proposed dynamic range are problematic.

The approach described here adjusts the optical properties of the used particle material to the measurement problem and therefore increases the size range sensitivity of a typical PDA measurement setup to a dynamic particle diameter range of approximately 1:200 (Fritsching et al., 1995). Thus, small tracers and bigger particles can be measured simultaneously which are discriminated directly by the detected phase difference without overloading or destroying the detectors by excessive scattered light intensities of bigger particles.

In a tracer/particle flow relatively short tracer signal lengths with poor signal quality (the intensity exceeds the noise only insufficiently) exist next to long particle signal lengths with high amplitude. If the quality of the tracer signals is poor, usual measurement systems identifying signals exceeding a critical trigger level, produce a number of incorrect measurements of the tracer signals. Due to this the detected diameter distributions of the tracer particles are measured broader than expected. This effect is extremely increased for high tracer concentrations in the flow

field which are necessary to detect the velocity distribution in the flow nearly continuously (high frequency detection). A dynamic trigger or additional validation criteria may result in more exact measurements but extend the signal processing effort and by this decrease the data acquisition rate. This is inconsistent with the requirement for analysis of turbulent flows where a detection of rapid turbulent velocity fluctuations is necessary.

For detailed analysis of turbulence modulation effects in a two-phase dispersed flow an extension of the size range sensitivity and the development of a suitable signal processing system are necessary. Here reliable signal processing of poor signals, where the burst amplitude is almost of the magnitude of the noise or below, and fast detection of the rapid velocity fluctuations of a turbulent flow are needed.

2. Increasing the sensitivity of the PDA

2.1. Parameters of the PDA system

Based on the Mie scattering theory, the scattered light field of a typical PDA setup (Bauckhage, 1988; Bauckhage et al., 1988) is derived by means of a numerical simulation routine (Jiang, 1994). The set of constant parameters for the development of the PDA is described in Table 1.

The parameters for setup optimisation are: the polarisation angle of the incident beam, the off-axis and elevation angles of the detectors and the complex refractive index n of the particles

$$n = a - \kappa \mathrm{i}$$

consisting of refractive index a (real part) and absorption index κ (imaginary part).

2.2. Determining the particle characteristics

The light scattered by a particle consists of reflected, different order refracted and diffracted parts. Only if reflection or refraction dominates, the phase difference to diameter correlation of a PDA measurement is linear as known from geometric optics. When measuring transparent solid particles in a forward scattering direction, the refractive part of the scattered light dominates. A direct determination of the particle diameter is possible, but as the scattered light intensity increases with the particle diameter squared in the particle size range under investigation and due to

Table 1
Fixed parameters of PDA arrangement

Laser wavelength	514 nm
Incident beam distance	65 mm
Front lens focal length	1200 mm
Incident beam power	250 mW
Receiver focal length	600 mm
Aperture geometry	Circular
Photodetector diameter	50 mm

limited photomultiplier sensitivity, the detectable measurement range for the particle diameter is limited to approximately 1:30.

For light absorbing particles, the amount of refracted light is extremely limited or completely eliminated in the forward scattering direction. Therefore, by arrangement of a specific composition of the optical particle characteristics for bigger particles, the detectable measurement range can be expanded (Gillandt et al., 1998).

Fig. 1 shows the calculated scattered light intensity for spherical glass beads, depending on the particle diameter for different absorption rates κ. Intensity values are normalised with respect to the light intensity a tracer particle (1 μm) scatters. The simulations are carried out for parameters of a conventional two detector PDA setup (off-axis angle $\varphi = 40°$, elevation angle $\psi = 1.7°$, parallel polarisation). This configuration is close to the measurement parameters of the experimental investigations derived finally and described later.

The scattered light intensity increases with particle diameter. For transparent particles ($\kappa = 0$), the scattered light intensity of a 50 μm particle is 2500 times bigger than the scattered light intensity of a tracer (which is the conventional limit of a photomultiplier dynamic range). The result of increasing absorption rates is a decreasing scattered light intensity. An absorption rate of $\kappa = 0.002$ is already sufficient to limit the scattered light intensities into the limits of the photomultiplier dynamic range.

The use of absorbing particles reduces the scattered light intensity of the particles and due to this simultaneous detection of small tracers and particles in a diameter range of approximately 1:200 is possible.

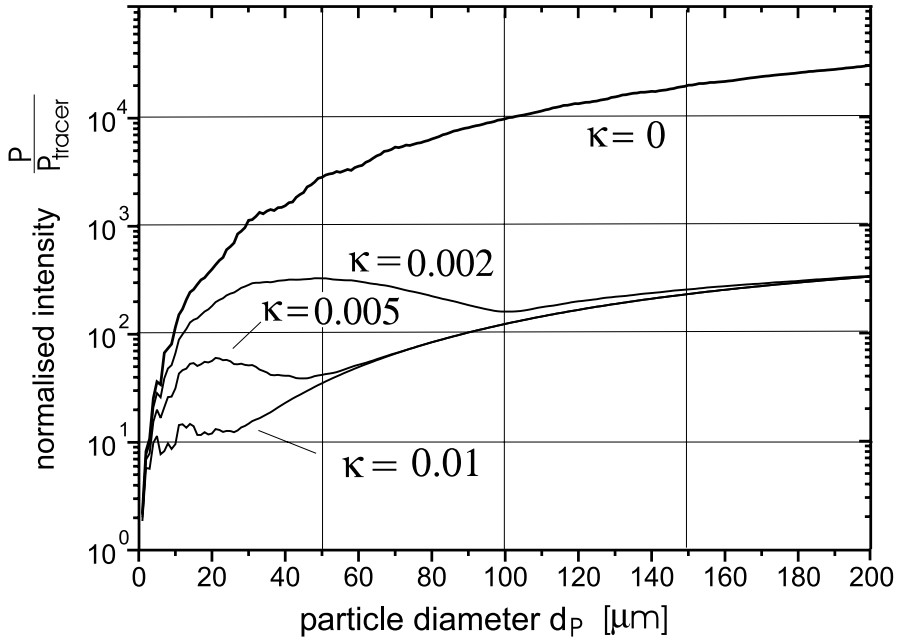

Fig. 1. Scattered light intensity of glass particles dependent on particle diameter d_p and absorption rate κ.

Despite the limited light intensity, also a linear (at least monotonic) behaviour of the phase difference to diameter relation is necessary for PDA measurements. Fig. 2 describes the calculated phase difference dependent on particle diameter for the conditions described before. For transparent particles ($\kappa = 0$), the refracted part of light dominates and the relation between particle diameter and phase difference is linear. The phase difference is negative. For small absorption rates ($\kappa = 0.002$), refraction dominates for $d_p < 90$ μm and reflection dominates for particle diameters $d_p > 150$ μm. Between these two linear functions refraction and reflection are of the same order and the behaviour of the phase difference changes from the linear refraction function to the linear reflection function (for $d_p = 90, \ldots, 150$ μm). The phase difference/diameter relation is not monotonic. At absorption rates $\kappa > 0.005$ the diameter range where reflection and refraction are of the same order is shifted to smaller particle diameters and the phase difference/diameter relation is linear for particle diameters bigger than $d_p = 60$ μm. In this particle diameter range, simultaneous measurement of tracers ($d_T \approx 1$ μm) and particles ($d_p > 60$ μm) is possible with a standard PDA setup.

Based on the results described above, an absorption rate of $\kappa = 0.009$ has been selected for the particles used here. This absorption rate was realised by colouring the particle material homogeneously with Fe_2O_3 and CoO (Fritsching et al., 1995). These particles are produced by spheroidisation of crushed glass particles from a coloured glass frit. For the especially manufactured particles, the size distribution and sphericity of the particles were controlled by scanning electron microscopy (SEM) and the complex refractive index of the material was measured by ellipsometry.

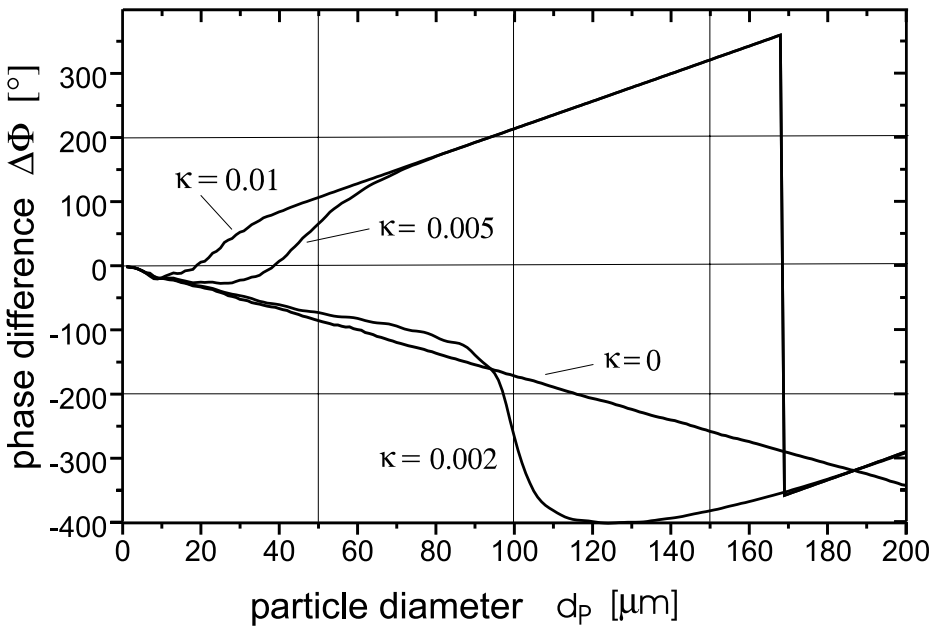

Fig. 2. Phase difference $\Delta\Phi$ of glass particles dependent on particle diameter d_p and absorption rate κ.

3. Optimising the geometrical PDA arrangement

In Fig. 3 the scattered light intensity versus off-axis angle of the photomultipliers is shown for 100 μm particles and 1 μm tracers for perpendicular and parallel polarisation of the incident beams. The tracer scattered light intensity decreases extremely for increasing off-axis angles and so detection at forward scattering angles is a basic requirement. For parallel polarisation at the off-axis angle of 67°, the detectable light intensity ratio is the best (≈2). This is the Brewster angle where no reflection occurs. At this angle the photomultiplier still receives some light scattered by a particle because of the integrating behaviour due to the finite receiving optics size. Although the light intensity ratio is best at 67° the total light intensity received at this position is not sufficient for measurements with the described PDA system. For these measurements the off-axis angle of 40° is chosen because of a sufficient light intensity ratio combined with a sufficiently high total tracer light intensity.

For a given particle diameter range the phase difference increases with increasing elevation angles. For measuring particle diameters even smaller than 160 μm, an elevation angle of $\psi = 1.7°$ has to be chosen. Due to the finite size of the detectors the photomultipliers have been arranged in a staggered arrangement (see Table 2), which has been described in detail in a previous publication (Gillandt et al., 1998).

Fig. 4 shows the scattered light intensity and phase difference for tracers and particles dependent on particle diameters from 0 to 160 μm within the realised setup. The maximum light intensity ratio between particles and tracers is 170 which is easily detectable by conventional

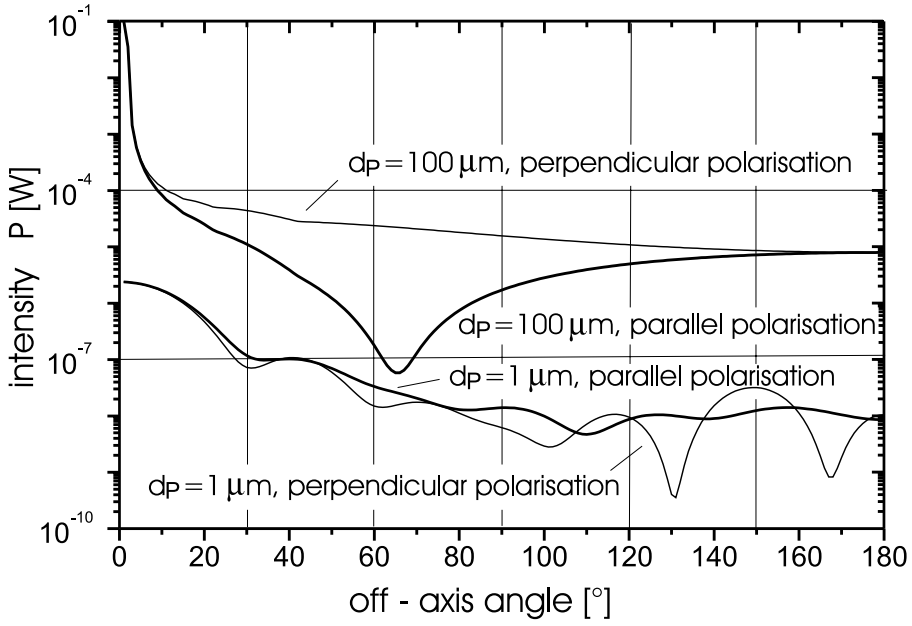

Fig. 3. Scattered light intensity versus off-axis angle for 100 μm particles and 1 μm tracer particles for different polarisation angles.

Table 2
Receiver positions in the experimental setup

	Receiver 1	Receiver 2
Distance to measuring volume (mm)	685	695
Off-axis angle (°)	40.5	38
Elevation angle (°)	1.7°	−1.7°

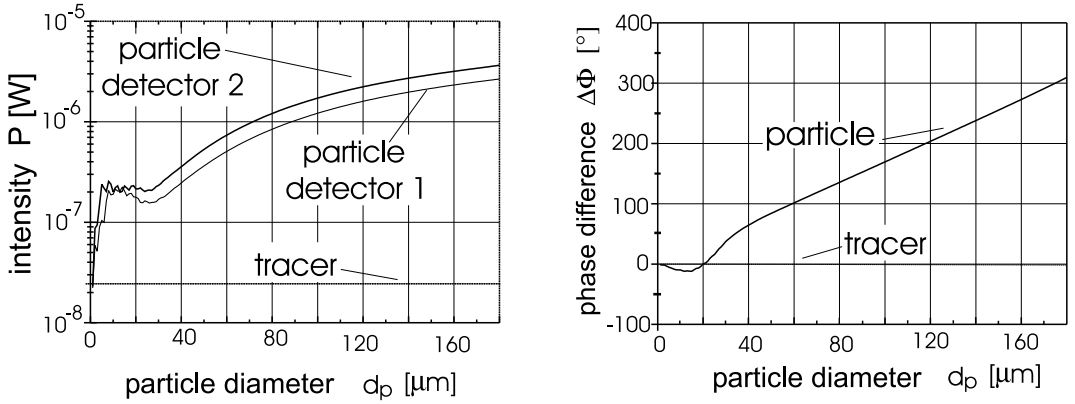

Fig. 4. Scattered light intensity and phase difference for the realised setup.

photomultipliers. Due to the staggered receiver positions, the phase difference to diameter relation is not linear but monotonic for particles $d_p > 20$ μm which has to be considered during measurements. As the finally used geometric setup with the staggered detector arrangement differs from the conventional arrangement previously calculated in Fig. 2, the gradient of phase difference to diameter relation is not exactly the same as shown in Fig. 2. Therefore, the jump of the phase difference for the particle size $d_p = 170$ μm seen in Fig. 2 is absent in Fig. 4.

4. Signal processing

Due to the poorly scattered tracer light intensity (scattering light ratio: particle/tracer ≈ 200) detection of the tracer signals is extremely disturbed. This proneness to disturbances of the poor tracer signals (resulting in diameter distributions broader measured than expected) needs to be reduced by a higher signal quality or additional signal validation criteria (Gillandt et al., 1998).

For nearly continuous measurements of the gas velocity the discrete tracer particles have to be detected in time intervals as small as possible. Due to the high tracer concentration necessary for this, the optical behaviour of the flow becomes more dense and therefore the light scattered from individual tracer particles in the measuring volume may be disturbed by multiple scattering from particles outside of the measurement volume. Due to the resulting poor signal quality in highly loaded tracer flows, the highest tracer amount to be used within usual PDA or LDV systems is limited (Strakey et al., 1998). To enable nearly continuous velocity measurements even at high

tracer concentrations in the two-phase flow a special signal processing procedure is developed for the measurements described here. The aim of this algorithm is to produce sufficient results in spite of poor signal quality.

In Fig. 5 a part of a continuous signal band detected about 1000 sampling points is shown as received from one photomultiplier. In this signal sequence the highest amplitude of the particle signals is limited to a certain maximum value. In the left and middle part of this sequence no clear signals can be identified directly from the signal amplitude distribution. At the right-hand side of the sequence a signal can be distinguished from (white) noise. This burst emerges clearly above the noise and can be distinguished clearly from the signal band by using the signal amplitude. Due to its high amplitude this signal is identified as a particle signal in all probability. The aim of the following signal processing algorithm is to identify even poor tracer signals which are hidden in such a signal band.

In general, PDA-bursts are detected by setting proper trigger criteria to distinguish the bursts from the noise (Ruck, 1987). For this, the burst amplitude often is used as a trigger criteria and the signal processing is done on-line when a burst is identified. With this signal processing routine sufficient results are developed when the bursts emerge clearly above the noise and can be identified easily from the signal band by using the signal amplitude. In contrast to this typical on-line signal processing, in the present contribution the signals are evaluated off-line (Tillwick et al., 1999). About a prescribed time interval a digitised signal band is completely recorded including bursts as well as noise (see Fig. 6). The length of the signal band is limited to 10 million samples (by the memory of the present A/D converter

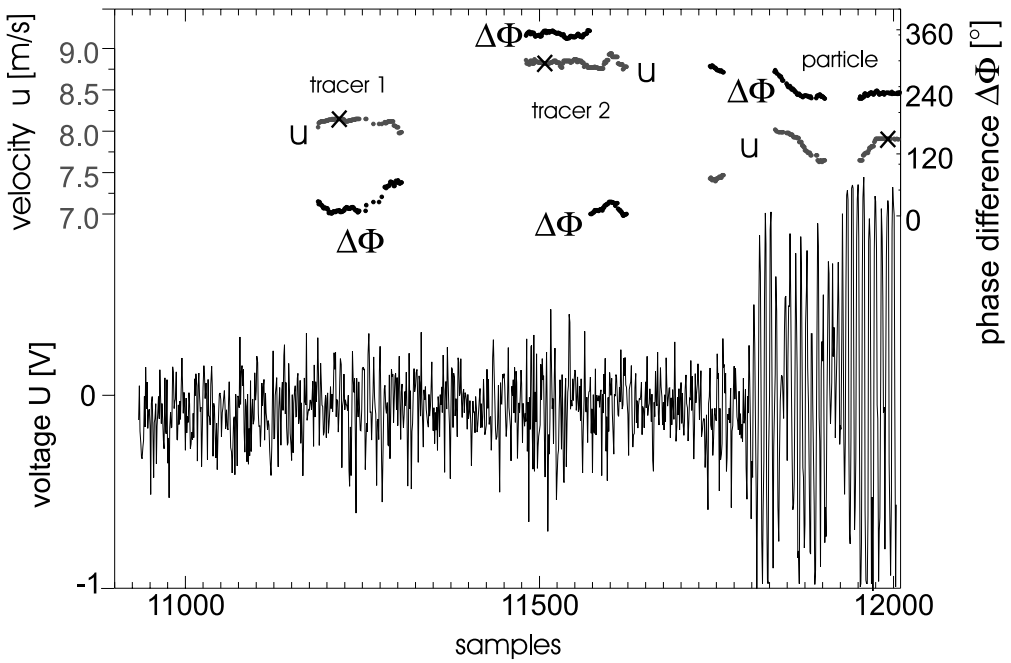

Fig. 5. Part of a signal band received from one photomultiplier.

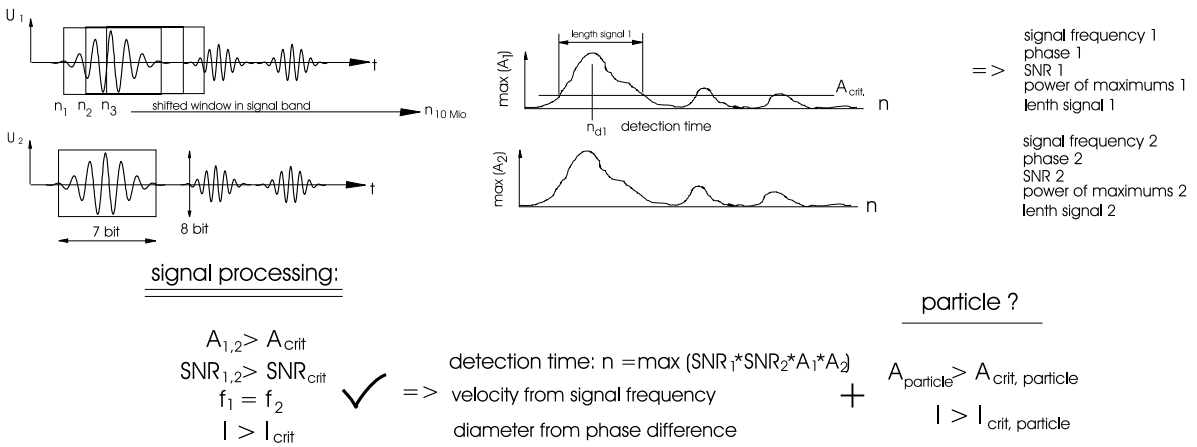

Fig. 6. Signal processing procedure.

board). With sampling frequencies in the range 1–6 MHz (which is dependent on the expected local velocities) the length of the detected signal band in time varies from 1 to 10 s. This signal band is stored without any data evaluation. The data evaluation (post-processing) is done in a second step off-line. Therefore, the amplitude spectrum of the whole signal band is calculated by fast-Fourier-transformation (FFT) in the vicinity (of a window of about 128 sampling points) of each signal band sampling point. As a result of this FFT, the amplitude of the highest frequency is shown in Fig. 5. In the amplitude spectrum of the FFT the tracer signals can be identified because the power of pure white noise spreads over a wide range (because it consists of random frequencies) whereas the power of the tracer signal bursts is mainly represented by just a single frequency.

A part of the signal band is accepted as a valid signal as long as the amplitudes a_1 and a_2 as well as the SNR ratios SNR_1 and SNR_2 are above their preset critical values and the highest frequencies of both detectors are identical (when the signals originate from the same particle). If this signal length is above a critical value l_{min} the detection time n is assumed to be the time where the product of the SNRs and amplitudes has reached the maximal value. At this point the velocity is calculated as analogous to a conventional PDA system.

Due to noise, some tracer signals may be not clearly identified as tracers ($\Delta\Phi = 0°, \ldots, 60°$ and $300°, \ldots, 360°$) but as particles ($\Delta\Phi = 80°, \ldots, 300°$). To eliminate such wrong measurements of tracer particles, only particle signals with $A_{particle} > A_{crit,particle}$ and $l_{particle} > l_{crit,particle}$ are evaluated as particles.

In addition to the amplitude of the signals, in Fig. 5 the velocity and phase differences are shown for areas where signals have been detected. The particle on the right-hand side of the signal (from sample 11 800 up) is detected at $\Delta\Phi = 240°$ and therefore $d_p = 140$ μm and $u = 7.7$ m/s. The phase differences and velocities in the first part of the particle signal (samples 11 800–11 950) show the proneness to disturbances even of bigger particles. In areas where the phase differences and velocities change continuously the signal cannot be evaluated. In the middle part of the signal two tracer signals are identified which have not been detected without the described post-processing algorithm.

5. Measurements in a two-phase jet

5.1. Generation of the two-phase jet

In order to analyse the turbulent structure in the two-phase flow, simultaneous measurements of tracers ($d_T = 1$ μm) and particles ($d_p = 60, \ldots, 160$ μm with $d_{p,50} = 110$ μm) have been carried out with the experimental setup of the particle laden jet illustrated in Fig. 7.

The gas flow is continuously seeded with tracer material – monosized spherical silica particles with a diameter of 1 μm (±10%) and a density of about 2000 kg/m^3. A constant particle mass flow rate is fed into the air flow by a feeder and injector system. Spherical glass beads with optical properties shown above have been used as particle material. The particle/gas flow discharges into ambient air through an accelerating tube with a diameter of $D = 12$ mm and a length-to-diameter ratio of 90. Since the PDA measurement volume is fixed at a certain point in space, the pipe is mounted on a two axis traversing system, allowing displacements of the whole jet system.

Below the measurement area the jet is collected by a funnel, operating at isokinetic conditions for non-intrusive collection of particles and tracers.

The particle size distribution as measured by PDA is shown in Fig. 8. Here the volume density distribution has been calculated from the PDA detected number density distribution assuming spherical particles. The mean diameter of the volume distribution is $d_{p,50} = 110$ μm. Comparing

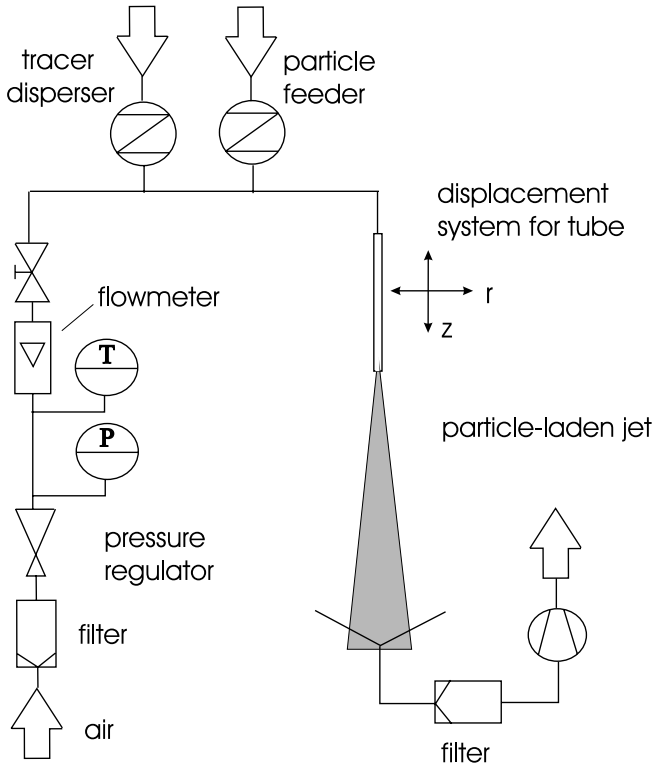

Fig. 7. Experimental setup for the two-phase jet.

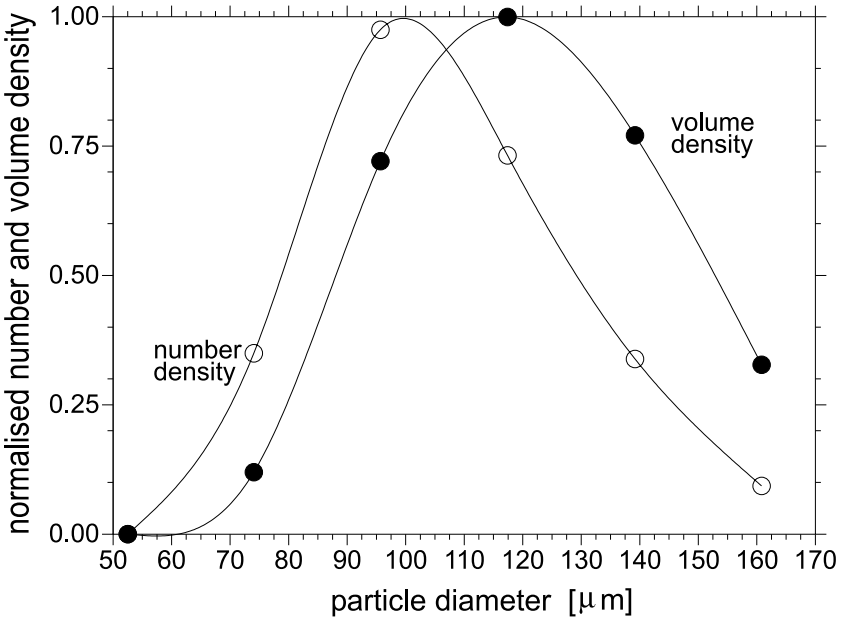

Fig. 8. Size distributions measured with PDA.

the volume density distribution of the PDA system with a laser-diffraction-spectrometry measurement has shown that the measured particle diameter distributions deviate by less than ±5% (Gillandt, 2000). In addition, the PDA measurement of a narrow particle size distribution resulting from sieve analysis resulted in an accuracy of ±5% of the PDA measured distribution (Gillandt, 2000). These comparisons illustrate the good quality of particle size detection of the PDA system (which is more critical than the velocity measurement).

6. Results and discussion

Measurements have been performed in the developing and self-similar region of the two-phase jet close to the nozzle.

Fig. 9 shows the axial profiles of the measured mean velocity and turbulence intensity in the centre of the jet for the single-phase jet compared to the two-phase jet (measurement conditions are given in Table 3). The velocity profiles are normalised by the mean velocity in the centre of the nozzle exit ($u_0 = 7.7$ m/s). The mean velocity of the two-phase jet at the edge of the profile is reduced to be less compared to the single-phase jet. In the whole jet flow centre turbulence intensity of the two-phase jet is lower than that for the single-phase jet. In the initial region ($z < 70$ mm) the single-phase flow turbulence intensity increases from 4.5% up to 15% for higher axial distances to the nozzle due to the influence of the outer shear layer. At the nozzle exit turbulence intensity is low in the centre of the flow. In the shear layer production of turbulence kinetic energy is high (which is described later) and due to radial turbulence transport from the outer shear layer into the centre of the jet turbulence intensity is increased in the centre of the

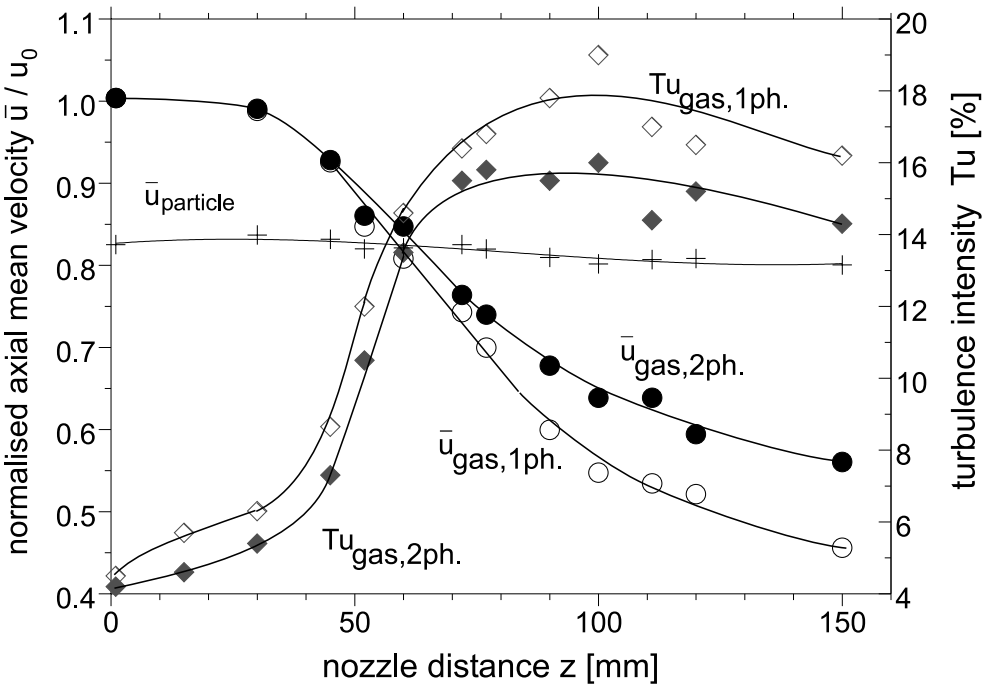

Fig. 9. Axial profiles of mean velocity and turbulence intensity in the centre of the single- and two-phase jet.

Table 3
Measurement conditions

Reynolds number	5700
Tube diameter	12 mm
Particles	Glass beads
Mean particle diameter	110 μm
Mass loading	1

initial region. In the initial region turbulence intensity reduction due to the dispersed particles in the two-phase jet is nearly constant at 0.5%. This turbulence intensity reduction seems to be independent of the increasing local turbulence intensity in the centre of the initial region.

In the (nearly developed and) developed jet region ($z > 70$ mm) a low decrease of turbulence intensity for increasing distances to the nozzle is observed in the centre of the jet. Reduction caused by particles is bigger than the value in the initial region though the local mass flux in the centre of the jet is lower in the developed jet than in the initial jet region (Fig. 10, mass flux profiles). If turbulence is reduced only by turbulence energy transfer from eddies to particles (following the eddies), the reduction of turbulence should be lower with decreasing mass flux (at constant *Tu* values in the single-phase jet). But the measured turbulence intensity reduction shown in Fig. 9 is different. It is low in the initial region of the jet flow where mass flux is high in the centre of the jet and much bigger in the developed jet where mass flux is lower in the centre of the jet.

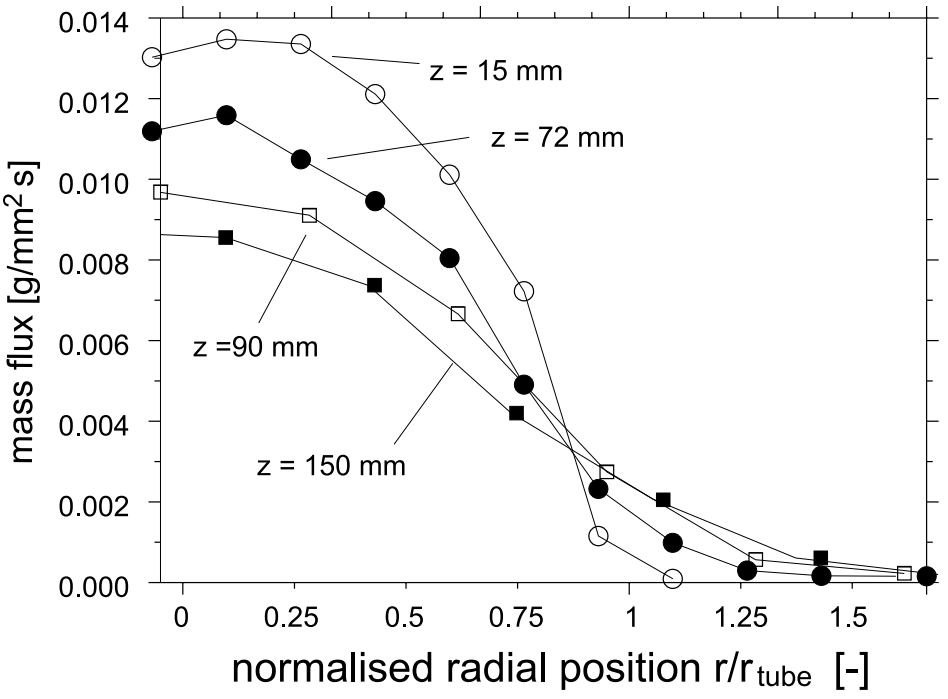

Fig. 10. Mass flux profiles in the two-phase jet.

The reason for the differences in turbulence intensity reduction due to particles seems to be the result of different effects decreasing turbulence in the two-phase jet flow. To understand the driving effects reducing turbulence in two-phase jet, different flow situations are investigated in detail for different radial profiles.

Fig. 11 shows the measured axial time-averaged mean, RMS fluctuating velocities (normalised with the single-phase gas velocity in the centre of the nozzle exit) and turbulence intensity of single-phase jet compared to the two-phase jet for radial profiles at various axial distances to the nozzle. The flow is axisymmetric in principle and because of this the profiles shown describe the velocity field at the nozzle distances measured. Tracer particles were seeded into the jet flow only (as shown in Fig. 7) and not into the surrounding flow regions. Due to this, the tracer concentration in the centre of the jet is high (each point in Fig. 9 and in the centre of the jet in Fig. 11 represent more than 20 000 individual measurements) and is reduced towards the boundary of the jet. As a result of this tracer concentration reduction the quality of the gas velocity measurements at the very outer boundary of the jet is lower compared to that in the centre of the jet. For the present turbulence modulation measurements the area with high particle concentration is of special interest and in this area the tracer concentration is sufficient. Results of gas velocity measurements at the very outer boundary of the jet are out of interest here.

At the nozzle exit ($z = 1$ mm) a typical velocity profile for single-phase tube flow is observed. Velocity reaches its maximum at the centre of the flow ($r = 0$ mm) and is reduced near the wall ($r = r_{\text{tube}}$). In the two-phase jet the mean axial velocity profile of continuous phase is nearly the same as the single-phase jet's profile.

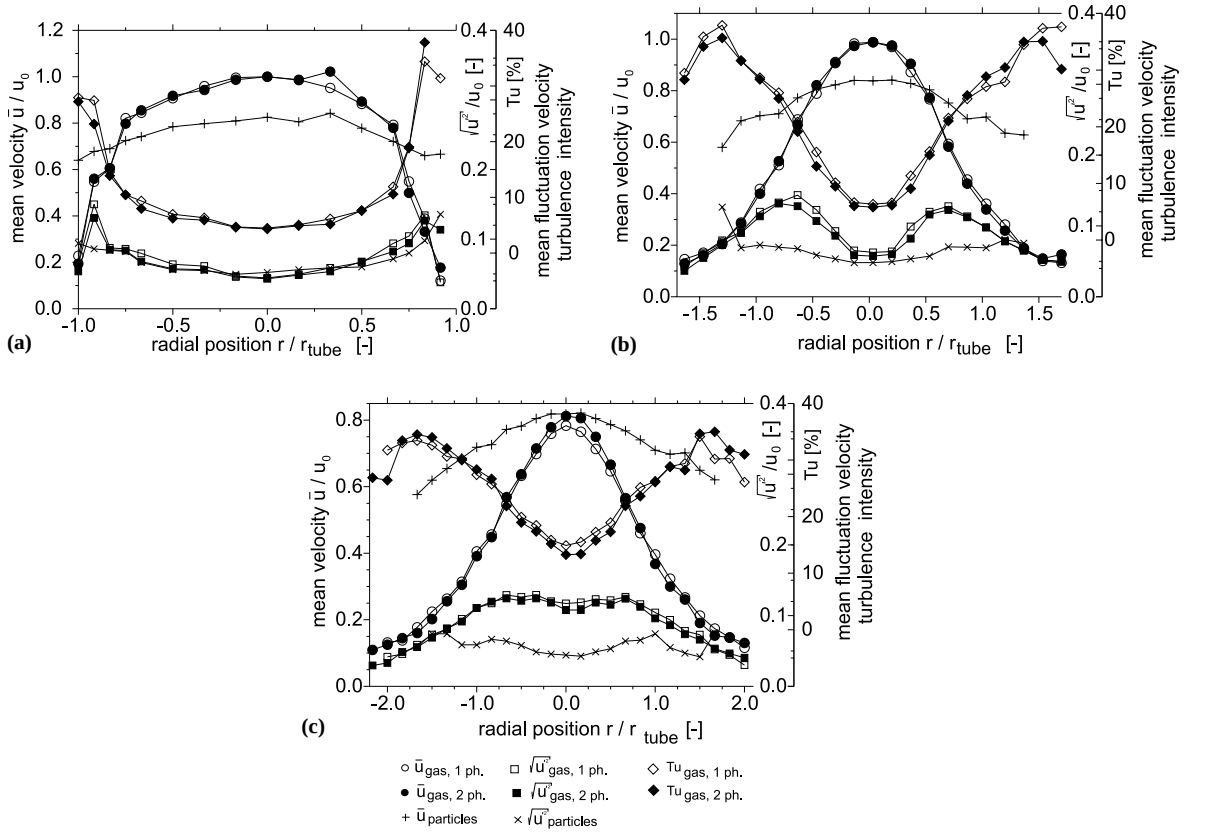

Fig. 11. Radial profiles of mean velocity, velocity fluctuations and turbulence intensity of single- and two-phase jet in the initial region: (a) $z = 1$ mm, (b) $z = 30$ mm and (c) $z = 60$ mm.

Collisions at the tube wall and the insufficient acceleration length of the tube entail that the dispersed phase velocity is almost steady at a constant value of 0.8 of the gas velocity in the centre of the profile. (Particle velocities shown in the figures here result from the particle class $d_p = 95$ μm (which is the peak in the number density distribution shown in Fig. 8)). This particle class is representative for all the other particle velocities. This particle velocity is lower compared to the continuous phase velocity in the centre of the flow, but higher than the continuous phase velocity in the wall region.

At the tube exit the fluctuations of gas velocity u_{rms} in the single-phase jet are low in the vicinity of the centreline ($Tu = 4\%$) and increase radially towards the shear layer at $r = r_{tube}$ ($Tu = 30\%$). The particles in the two-phase jet have no influence on the turbulence intensities in the centre of the flow. In the shear layer, u_{rms} is lower for the two-phase jet in this area resulting in a lower turbulence intensity in comparison to single-phase flow.

At distances of $z = 30$ and $z = 60$ mm below the nozzle, the gas velocities show typical jet flow profiles. In the shear area of the two-phase flow, particle velocities are higher than the gas velocity because of the mass inertia of the particles. Due to momentum transfer from the particles to the fluid in the shear area, the velocity of the gas phase is higher at $z = 60$ mm, which results in a

lower spreading rate and higher gas velocities in the whole profile of two-phase jet in comparison to single-phase jet. The fluctuation velocities of the single-phase flow are highest at positions within the shear layer with highest velocity gradients (e.g., $z = 60$ mm, $r = 2/3r_{\text{tube}}$: $Tu = 20\%$) and decrease towards the centreline (e.g., $z = 60$ mm, $r = 0$: $Tu = 15\%$) as well as towards the boundary of the jet (due to low gas velocities in this area). In the centre of the initial region the gas turbulence increases with increasing distances to the nozzle for the single- and the two-phase flow situation (which is described in Fig. 9). The reason for increased turbulence is high radial diffusive turbulence transport from the shear layer into the centre of the flow.

In the two-phase jet the velocity fluctuations (and the turbulence intensities) are reduced in comparison to the single-phase jet. At the nozzle distance of $z = 30$ mm the turbulence reduction in the two-phase jet is highest in the area between the centre of the jet and the high velocity gradient. At $z = 60$ mm the turbulence intensity reduction is highest in the centre of the jet. This development of turbulence intensity reduction mainly results from reduced radial turbulence transport in the two-phase flow.

The reason for the reduced radial turbulence transport cannot be explained only based on the analysis of local statistical values as shown in Figs. 9 and 11. Analysis of the local turbulence structure in the flow field is necessary.

At $z = 30$ mm time averaged mean velocities of single- and two-phase jets have almost the same values. Due to this changes of turbulence structure cannot be influenced by different profiles of single- and two-phase jets. The procedure for obtaining energy density spectra from measured gas velocity signals has been described in Gillandt and Fritsching (1999).

The one-dimensional energy spectra of the axial velocity fluctuations for the single- and two-phase jet flows are shown in Fig. 12 at $z = 30$ mm distance to the nozzle exit in the centre of the jet ($r = 0$ mm) and in the shear layer ($r = 4$ mm) where turbulence is mainly produced. Results for

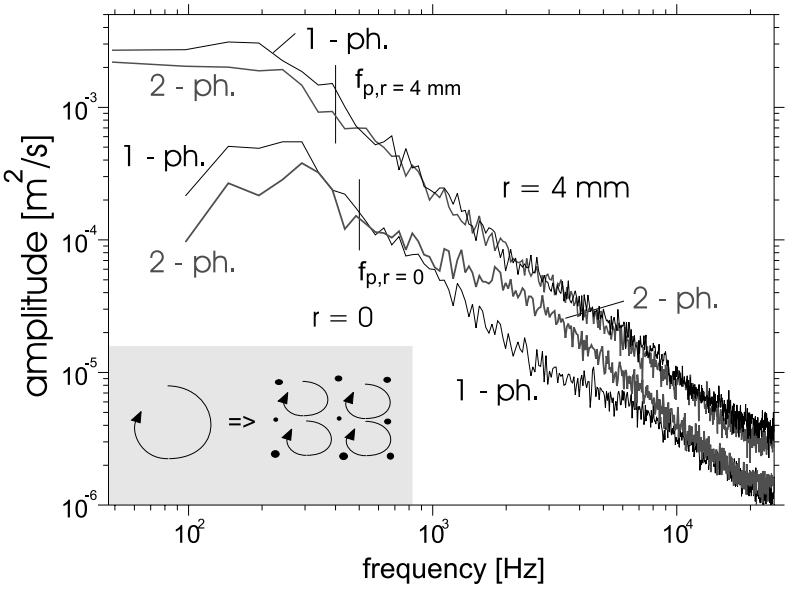

Fig. 12. Energy spectra of the axial velocity fluctuations for single- and two-phase jet at $z = 30$ mm.

the energy spectra show the typical behaviour in turbulent flow as constant intensities within frequencies of large eddies (small frequencies) in the shear layer at $r = 4$ mm. In the centre of the jet a maximum fluctuation resulting in Strouhal numbers $Sr \approx 0.38, \ldots, 0.45$ (which is based on shear layer instabilities at the nozzle exit) can be observed (Nieberle, 1987) at small frequencies. At high frequencies in the shear layer and in the centre of the jet there is a decrease of growing frequencies (small eddies) in the dissipation range with a constant slope of −5/3 (Tennekes and Lumley, 1990).

As a result of the limited signal length and restricted time resolution (approximately 20 000 samples/s) frequencies in the range 100 Hz $< f < 5 \times 10^3$ Hz are reliable.

Intensity of all frequencies in the energy spectra is higher in the shear layer than in the centre of the jet. In the shear layer area with highest velocity gradients, turbulence production is highest. In the two-phase flow, intensity at low frequencies (large eddies) is less compared to the single-phase jet, whereas the intensity at large frequencies (small eddies) seems to be higher in the centre of the single-phase flow.

The derived frequency resulting from the interparticle spacing f_p of the particles is marked in the frequency spectra shown in Fig. 12. This characteristic frequency has been calculated from a number concentration-based mean interparticle spacing and the particle mean velocity. In the two-phase jet shear layer the intensity of eddies larger than this mean particle distance is reduced.

Owing to the presence of dispersed particles in the flow, large eddies seem to disintegrate into smaller eddies as shown in principle in the lower left of Fig. 12. Because the mobility of large eddies is restricted by the dispersed particles, the eddy seems to disintegrate into smaller eddies which can move more easily in the spacing between the particles.

The smaller turbulence in the centre of the two-phase jet (compared to the single-phase jet) due to reduced turbulence transport identified in Figs. 9 and 11 seems to be a consequence of the turbulence structure change with smaller intensities of large eddies. Furthermore this disintegration of large eddies causes turbulence intensity reduction.

Fig. 13 illustrates the mean velocity, fluctuation velocity and turbulence intensity for the single-phase jet compared to the two-phase jet for radial profiles in the developed region of the jet (at nozzle distances $z = 90$ and $z = 150$ mm). While the decrease of turbulence is caused mainly by reduced radial turbulence transport in the initial region of the two-phase jet radial turbulence transport in the developed jet flow is lower because of a low velocity fluctuation (and *Tu*-) gradient. The fluctuation of gas velocity u_{rms} is highest and almost constant in the centre of the developed jet flow and decreases for increasing radial positions. While fluctuation velocities of single- and two-phase jet have the same values at the beginning of the developed jet (at $z = 90$ mm), at larger distances to the nozzle ($z = 150$ mm) the velocity fluctuation is higher in the two-phase jet than in the single-phase jet. As a result of a much higher mean velocity in the two-phase jet a reduction of turbulence intensity owing to the presence of particles in the centre of the jet can be observed (comparing profiles at the same distance to the nozzle). Due to the lower radial turbulence transport in the developed jet, the turbulence transport along the jet axis becomes more and more important for higher nozzle distances and with it the time turbulence influenced by dispersed particles seems to increase. This could be the reason for higher turbulence intensity reduction in the developed jet region.

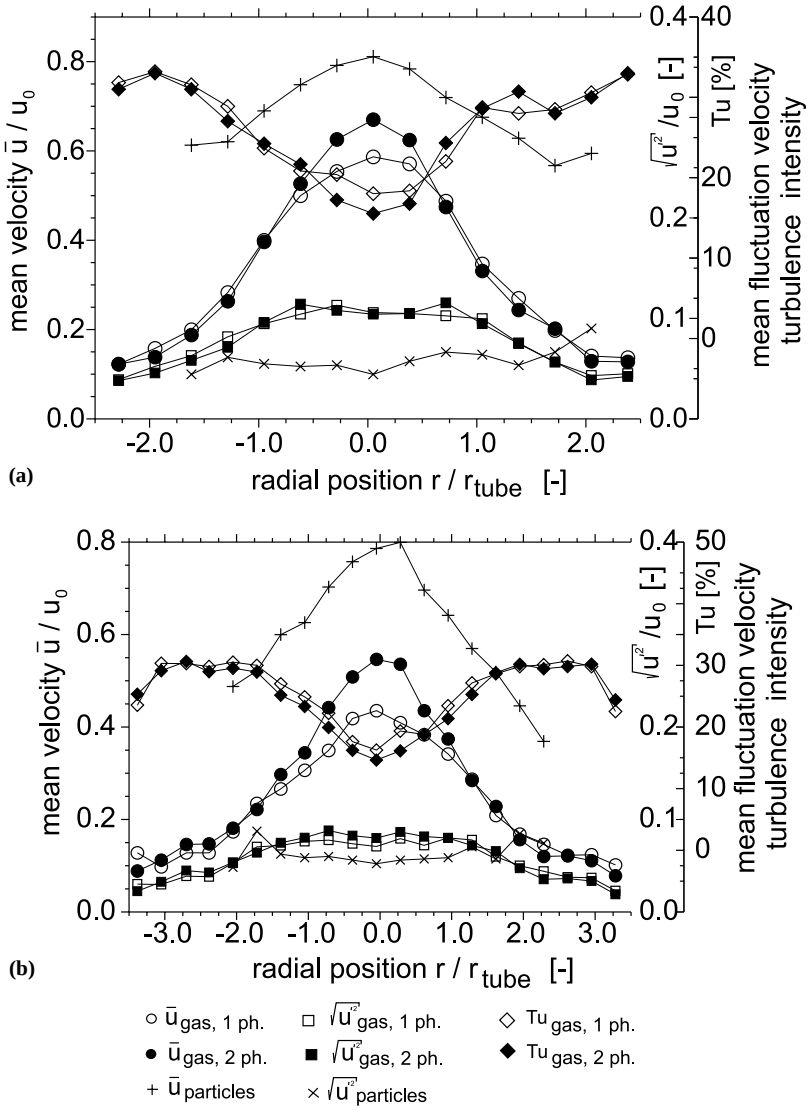

Fig. 13. Radial profiles of mean velocity, velocity fluctuations and turbulence intensity of single- and two-phase jet in the developed jet: (a) $z = 90$ mm and (b) $z = 150$ mm.

7. Conclusions

A method is proposed to increase the sensitivity of a PDA system allowing simultaneous size and velocity measurement of spherical tracers (for gas-phase detection) and particles in a diameter range from 1 to 200. The measurement approach has been applied successfully for simultaneous measurement of continuous and dispersed phase velocity profiles near the nozzle of a two-phase jet with a tracer to particle diameter range 1–160 μm. The local velocity distributions and turbulence structures of continuous and dispersed phases are investigated.

In a two-phase jet with Stokes numbers $St \gg 1$ different turbulence structure modification effects exist. The influence of these effects depends on the local position in the jet.

Near to the nozzle exit a high gas velocity gradient exists and a high turbulence production in the shear layer of the jet is observed. Here the turbulence in the jet depends on lateral turbulence transport. Due to a changed turbulence structure with reduced intensity of large eddies, the lateral transport in the two-phase jet is decreased compared to the single-phase jet in this area and therefore the turbulence intensity is decreased. In the area where the jet is nearly developed the velocity gradient in the shear layer is lower and due to this lateral turbulence transport effects no longer dominate the flow. Here turbulence transport along the jet axis becomes more important and the turbulence intensity reduction is higher. The turbulence modulation measured in the two-phase jet at $St \gg 1$ is generally low ($\Delta Tu/Tu < 20\%$).

References

Barlow, R.S., Morrison, C.Q., 1990. Two-phase velocity measurements in dense particle-laden jets. Exp. Fluids 9, 93–104.

Bauckhage, K., 1993. Phasen-Doppler-Anemometrie zum Bilanzieren und Modellieren mehrphasiger Strömungen. Chem.-Ing.-Tech. 8, 929–934.

Bauckhage, K., 1988. The phase-Doppler-difference method, a new laser-Doppler technique for simultaneous size and velocity measurement, part 1. Part. Part. Syst. Charact. 5, 16–22.

Bauckhage, K., Flögel, H.H., Fritsching, U., Hiller, R., 1988. The phase-Doppler-difference method, a new laser-Doppler technique for simultaneous size and velocity measurement, part 2. Part. Part. Syst. Charact. 5, 66–71.

Dopheide, D., Faber, M., 1989. In: B. Ruck (Ed.), Einsatz von Diodenlasern und Photodioden in der Strömungsmeßtechnik. AT-Fachverlag. Stuttgart.

Elghobashi, S.E., 1994. On predicting particle-laden turbulent flows. In: Proceedings of the Seventh Workshop on Two-Phase Flow Predictions.

Fritsching, U., Rheims, J., Wriedt T., Bauckhage, K., 1995. Use of homogeneously absorbing materials for research in dispersed multiphase flows. Int. Symp. on Meas. Techn. Mult. Phase Flow, Nanjing, China, 10–13, 4, 1995.

Gillandt, I., Schulze, T., Fritsching, U., Bauckhage, K., 1998. Simultaneous measurement of continuous and dispersed phase in a two phase jet flow. Flow Measure. Instrum. 9, 1–9.

Gillandt, I., Fritsching, U., 1999. Erweiterung eines PDA Systems zur Messung der Turbulenzmodulation im zweiphasigen Freistrahl. 7. Fachtagung: Lasermethoden in der Strömungsmeßtechnik, 27, -29.9.99, Saint-Louis, France.

Gillandt, I., 2000. Analyse der Turbulenzmodulation im dispersen zweiphasigen Freistrahl. Ph.D. thesis, University of Bremen, Shaker-Verlag, Aachen.

Gore, R.A., Crowe, C.T., 1989. Effect of particle size on modulating turbulence intensity. Int. J. Multiphase Flow 15, 279–285.

Hetsroni, G., Sokolov, M., 1971. Distribution of mass, velocity, and intensity of turbulence in a two-phase turbulent jet. J. Appl. Mech.

Hetsroni, G., 1989. Particles – turbulence interaction. Int. J. Mutiphase Flow 15, 735–746.

Jiang, Z., 1994. Theoretische Simulation der Phasen-Doppler-Anemometrie anhand der Mie-Theorie: Untersuchung an geeigneten Systemparametern. Ph.D. thesis, University of Bremen.

Jou, B.H., Shen, J.J., Lee, Y.T., 1993. Particle mass loading effect on a two-phase turbulent downwart jet flow. Part. Part. Syst. Charact. 10, 173–181.

Kulick, J.D., Fessler, J.R., Eaton, J.K., 1994. Particle response and turbulence modification in fully developed channel flow. J. Fluid Mech. 277, 109–134.

Lefebvre, A., 1989. Atomisation and Sprays. Hemisphere Publishing Corp, New York.

Nieberle, R., 1987. Entwicklung einer Methode der Mustererkennung zur Analyse kohärenter Strukturen und ihre Anwendung im turbulenten Freistrahl. Diss., VDI Fortschrittsberichte, Düsseldorf.

Prevost, F., Boree, J., Nuglisch, H.J., Charnay, G., 1994. Characerisation of a polydispersed particle-laden jet using a phase Doppler anemometer. Proc. ICLASS 94, Rouen, 938–945.

Qiu, H.-H., Sommerfeld, M., Durst, F., 1991. High resolution data processing for phase-Doppler measurements in a complex two-phase flow. Measur. Sci. Technol. 2, 455–463.

Ruck, B., 1987. Laser-Doppler-Anemometrie. AT-Fachverlag GmbH, Stuttgart.

Schreck, S., Kleis, S., 1993. Modification of grid-generated turbulence by solid particles. J. Fluid Mech. 249, 665–688.

Shuen, J.S., Solomon, A.S.P., Zhang, Q.F., Faeth, G.M., 1985. Structure of particle-laden jets: measurement and predictions. AIAA J. 23, 396–404.

Strakey, P.A., Talley, D.G., Bachalo, W.D., Breuer, A., 1998. Anwendung der Phasen-Doppler-Methode auf optisch dichte Sprays. Tagungsbeitrag Spray 98, 4. Workshop über Technik der Fluidzerstäubung und Erfassung von Sprühvorgängen, Essen, 13–14 October 98.

Tennekes, H., Lumley, J.L., 1990. A First Course in Turbulence. 13th printing, MIT Press, Cambridge, MA.

Tillwick, J., Uhlenwinkel, V., Bauckhage, K., 1999. Analysis of the spray forming process using backscattering phase-Doppler-anemometry. Int. J. Heat Transfer Fluid Flow 20, 530–537.

Tsuji, Y., Morikawa, Y., Tanaka, T., Karimine, K., Nishida, S., 1988. Measurement of an axisymmetric jet laden with coarse particles. Int. J. Multiphase Flow 14, 565–574.

Tu, J.Y., Fletcher, C.A.J., 1994. An improved model for particulate turbulence modulation in confined two-phase flows. Int. Commun. Heat Mass Transfer 21, 775–783.